Astron. Astrophys. 218, 231–240 (1989)

ASTRONOMY AND ASTROPHYSICS

Dust ring around λ Orionis

C.Y. Zhang [1,2,3], R.J. Laureijs [1,2], G. Chlewicki [1,2], F.O. Clark [1,4], and P.R. Wesselius [1]

[1] Laboratory for Space Research, P.O. Box 800, NL-9700 AV Groningen, The Netherlands
[2] Kapteyn Astronomical Institute, P.O. Box 800, NL-9700 AV Groningen, The Netherlands
[3] Purple Mountain Observatory, Academia Sinica, Nanjing, China
[4] Department of Physics and Astronomy, University of Kentucky, Lexington, KY 40506, USA

Received January 11, accepted November 21, 1988

Summary. Sky maps of a 12° × 12° region obtained by the Infrared Astronomical Satellite (IRAS) reveal a dust ring which has a diameter of about 9° and is centered on the H II region S 264 and its exciting star, λ Orionis. The 60/100 μm color temperature in the ring with an assumed dust emissivity law $\nu^{1.5}$ is on average 25 K. The luminosity in the IRAS wavelength range and the total far-infrared luminosity for the ring are 3.8 $10^4 L_\odot$ and 6.3 $10^4 L_\odot$ respectively. The radiation field responsible for the heating of dust in the ring contains an enhanced UV component with an energy density 2 to 3 times as large as that of the general interstellar radiation field. This enhancement of the UV component is ascribed to the O star λ Ori and several other early B stars. A careful analysis of the energetics of the ring shows that its total infrared luminosity can be explained by the energy supply from the λ Ori OB association, HD 34989 and the interstellar radiation field. The stellar radiation field from the λ Ori OB association dominates the heating of the H II region S 264.

Key words: infrared radiation – interstellar medium: dust – stars: pre-main sequence

1. Introduction

The H II region S 264 (Sharpless, 1959) is excited by the O8III ((f)) star, λ Orionis (Conti and Leep, 1974), which is a member of a small OB association (Murdin and Penston, 1977). Radio continuum mapping (Reich, 1978) of the Orion region shows that S 264 is ionization bounded with an electron density of 2.2 cm^{-3}. A dark ring surrounding the H II region was first recognized by Wade (1958). Denser portions of the ring were catalogued as dark clouds B30, B35, and B223 by Barnard (1927), who did not remark on the large scale structure. A ring is obvious in Khavtassi's (1960) map of absorption nebulae surrounding λ Ori. Optical extinction in the northeast quarter of this ring and in S 264 was obtained by means of star counts (Coulson et al., 1978).

Wade (1957, 1958) found a shell of neutral hydrogen which lies just outside S 264. CO emission was observed towards some of the dark clouds along the border of the H II region, e.g. B35 (Lada and Black, 1976). A ring of molecular gas is apparent in a large scale CO line ($J=1\rightarrow0$) survey of the Orion region (Maddalena et al., 1986; Maddalena and Morris, 1987, hereafter MM). MM interpret the CO data by suggesting an expanding ring inclined by 36°.4 with respect to the plane of the sky, thought to be a remnant of a flattened molecular cloud disrupted by the gas pressure within the H II region.

Duerr et al. (1982) surveyed for Hα emission objects in a region of about 100 square degrees centered on the λ Ori OB association, and detected 86 objects, of which 21 were not discovered by the earlier surveys. The majority of them have strong to medium Hα emission and are believed to be young, low to intermediate mass pre-main-sequence stars. Co-existence of the massive O stars and low-mass stars in this region indicates active star formation. Far-infrared properties of this prominent, nearby star formation region are investigated by us to obtain a better understanding of the relation between young stars and their surroundings.

A preliminary discussion of the IRAS data on the λ Ori shell was presented by Malone et al. (1987). Our analysis is much more detailed than in their study, and uses more refined data reduction techniques, essential in processing infrared measurements for an area as large as that of the λ Ori ring.

The analysis in this paper concentrates on the global infrared properties of the region (12° × 12°) surrounding λ Ori. Data and results are given in Sect. 2. The morphology of the infrared emission is described in Sect. 3. The energetics of both S 264 and its immediate environment are discussed in Sect. 4. Conclusions are given in Sect. 5.

2. Data and results

Infrared sky maps of the first IRAS sky survey (HCON1, IRAS Explanatory Supplement, 1985) of a region centered on λ Ori have been analyzed. Four sky maps were combined into a 17° × 17° image, in all four IRAS bands. Ecliptic and galactic background has been removed and the images have been destriped as described by e.g. Clark et al. (1986). After removing the ecliptic and galactic background a zero-level uncertainty of about 0.2 to 0.4 MJy/sr remains. The area used for background subtraction and destriping was larger than the actual region studied in the analysis of the λ Ori ring, which was a square of 12° × 12° centered at RA = $5^h34^m.1$, DEC = +9°55′ (1950). A grey-scale map with superimposed contours at 100 μm is shown in Fig. 1. A slightly

Send offprint requests to: C.Y. Zhang, Department of Physics, The University of Calgary, 2500 University Drive N.W., Calgary, Alberta, Canada T2N 1N4

elongated ring structure can easily be identified in the maps at all four IRAS wavelengths. The central region of the ring, containing the H II region S 264, also shows strong infrared emission. Several infrared peaks in the ring are associated with dark clouds and reflection nebulae (Fig. 2).

A diagram of the 60 versus 100 μm surface brightness for pixels in the ring clearly shows a strong correlation (Fig. 3). The slope of the regression line (0.23) corresponds to an average color temperature $T(60/100\,\mu m) = 25$ K (assuming blackbody emission modified by a dust emissivity law of $\nu^{1.5}$), which is somewhat larger than values found in diffuse clouds (Low et al., 1984; Boulanger et al., 1985; Weiland et al., 1986; Laureijs et al., 1987; Laureijs et al., 1988). In order to improve the signal-to-noise ratio of the color temperature map, the 60 and 100 μm maps were smoothed to a lower resolution with a gaussian beam of FWHM $15' \times 15'$ and regridded to a pixel size of $6' \times 6'$. Using the ratio of the smoothed maps the distribution of color temperature $T(60/100)$ has been derived and is shown in Fig. 4. The color temperature in S 264 varies from 26 K at the outer edge to 30–33 K close to λ Ori. A few spots in the ring, coincident with the dark clouds B35, B223, B31/32, B30, L1582/84, L1583 and B 225, have enhanced color temperatures of 26–27 K. The highest temperature in the ring is 30 K at the position of B223.

In order to derive the 100 μm optical depth, $\tau_{100\,\mu m}$, we have made the assumption that the 100 μm emission is optically thin, and that the dust grains are isothermal in the line of sight with a temperature distribution in the plane of the sky as shown in Fig. 4. The 100 μm optical depth can be calculated as $\tau_{100\,\mu m} = I_\nu / B_\nu(T)$, where I_ν is the intensity and B_ν is the Planck function. The resulting map of 100 μm optical depth is displayed in Fig. 5. The features visible in the $\tau_{100\,\mu m}$ map should be interpreted with caution: the apparent 60/100 μm color temperature, which is usually higher than the physical temperature of grains dominating the 100 μm emission (Terebey and Fich, 1986), was used in deriving $\tau_{100\,\mu m}$, and the temperature is not necessarily constant along the line of sight. The dust ring stands out clearly against its surroundings, whereas the H II region S 264 is hardly visible. The mean 100 μm optical depth in the ring is about $2.5\ 10^{-4}$ and the maximum value is $5.3\ 10^{-4}$. The opacity contrast between the ring and the H II region is a factor of 5 to 10. Since the observed infrared emission from the H II region tends to be dominated by the warmest dust close to λ Ori, the value of $\tau_{100\,\mu m}$ towards the center of S 264 excludes the cooler grains outside the H II region and may underestimate the true amount of dust. We conclude that the appearance of the ring is caused by enhanced dust particle density, while the relatively high surface brightness of the H II region is due to a temperature enhancement.

Diagrams in Fig. 6a and b show the variation of the surface brightnesses in all four IRAS bands, the optical depth $\tau_{100\,\mu m}$ and the integrated intensity of CO emission $W(CO)$ (taken from MM) along two cuts through λ Ori perpendicular to each other, whose directions are indicated by the lines AA′ and BB′ in Fig. 1, with

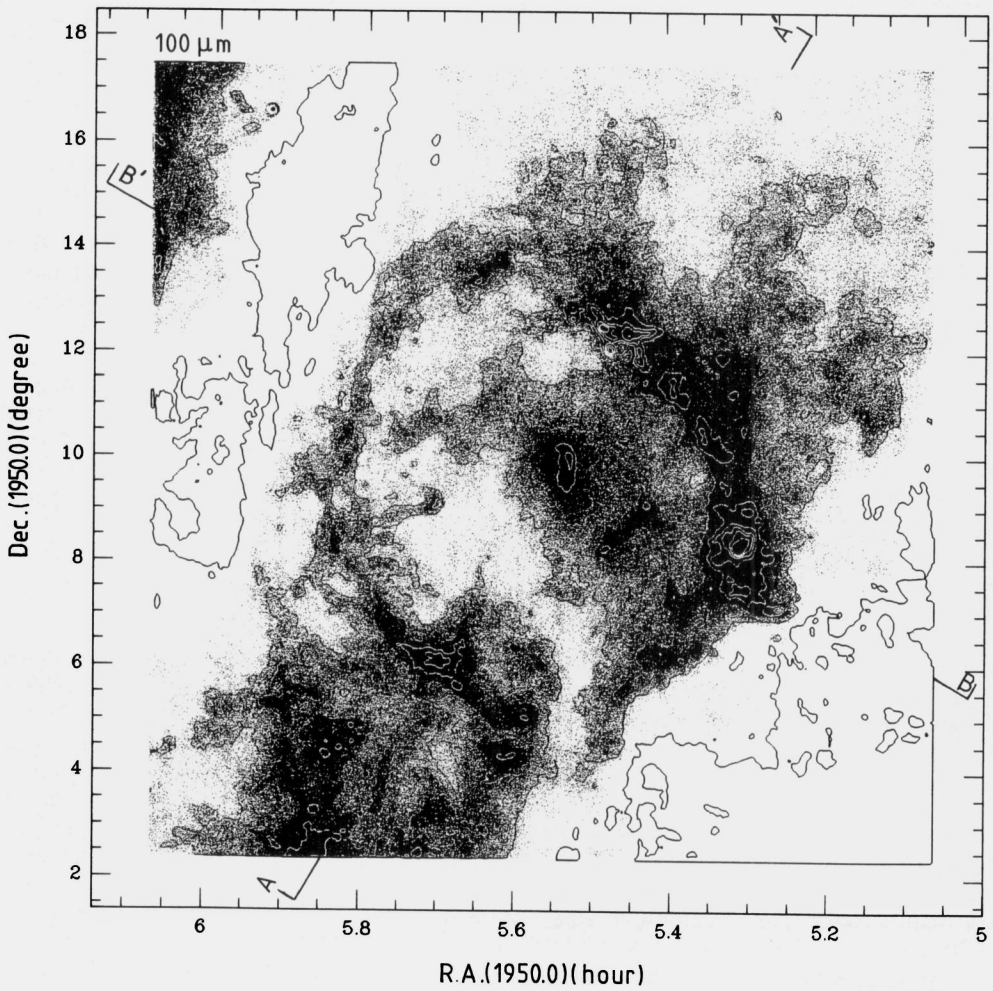

Fig. 1. Grey-scale image superimposed with contours at 100 μm of the λ Orionis Ring and the H II region S 264. The contour levels are 0, 10, 20, 35, 50, 65, 80 and 100 MJy/sr. The lines AA′ and BB′ correspond to the two cuts shown in Fig. 6a and b respectively

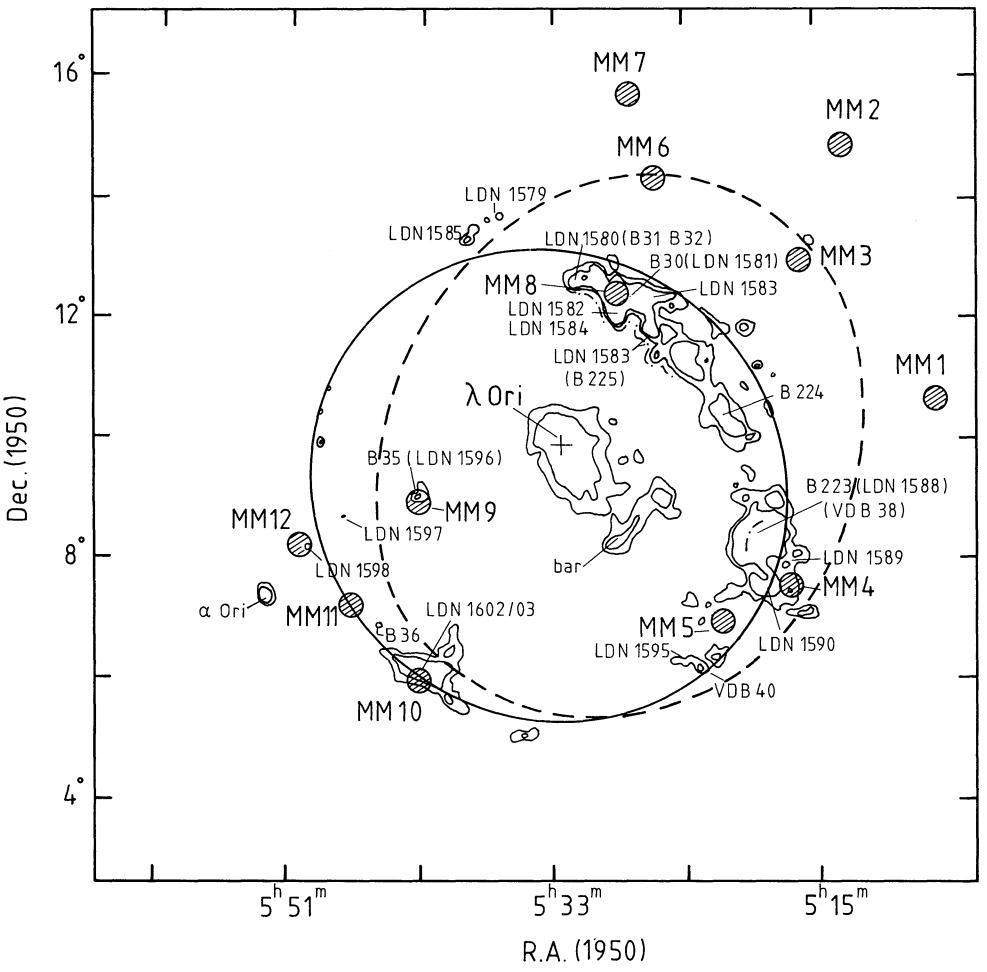

Fig. 2. Schematic diagram of the most prominent dust clouds of the λ Orionis ring. Contour levels are at 6 and 8 MJy/sr at 60 μm. Some clouds are labelled with the names of optically prominent objects. The solid ellipse indicates the dust ring; the dashed ellipse indicates the CO ring fitted to the positions and radial velocities of CO peaks designated by hatched circles (MM). Dash-dot lines are the positions of optically bright rims. A cross indicates the position of the star λ Ori. The infrared bar-like structure within the H II region S 264 is also indicated

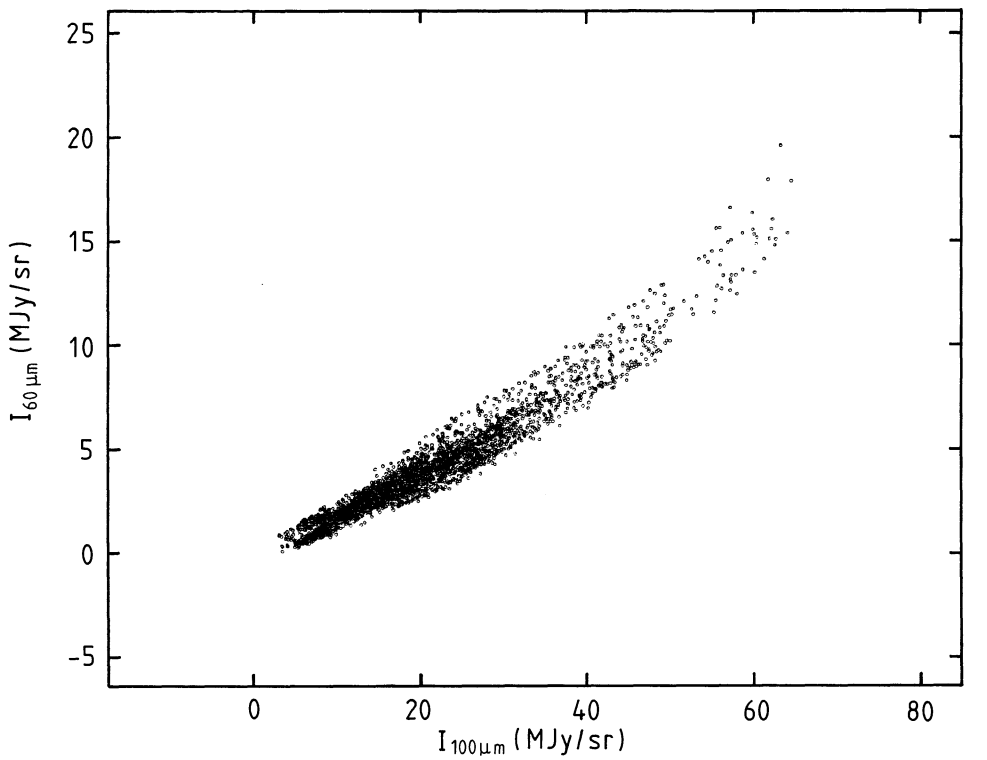

Fig. 3. Correlation between the 60 μm and 100 μm intensity of points in the ring

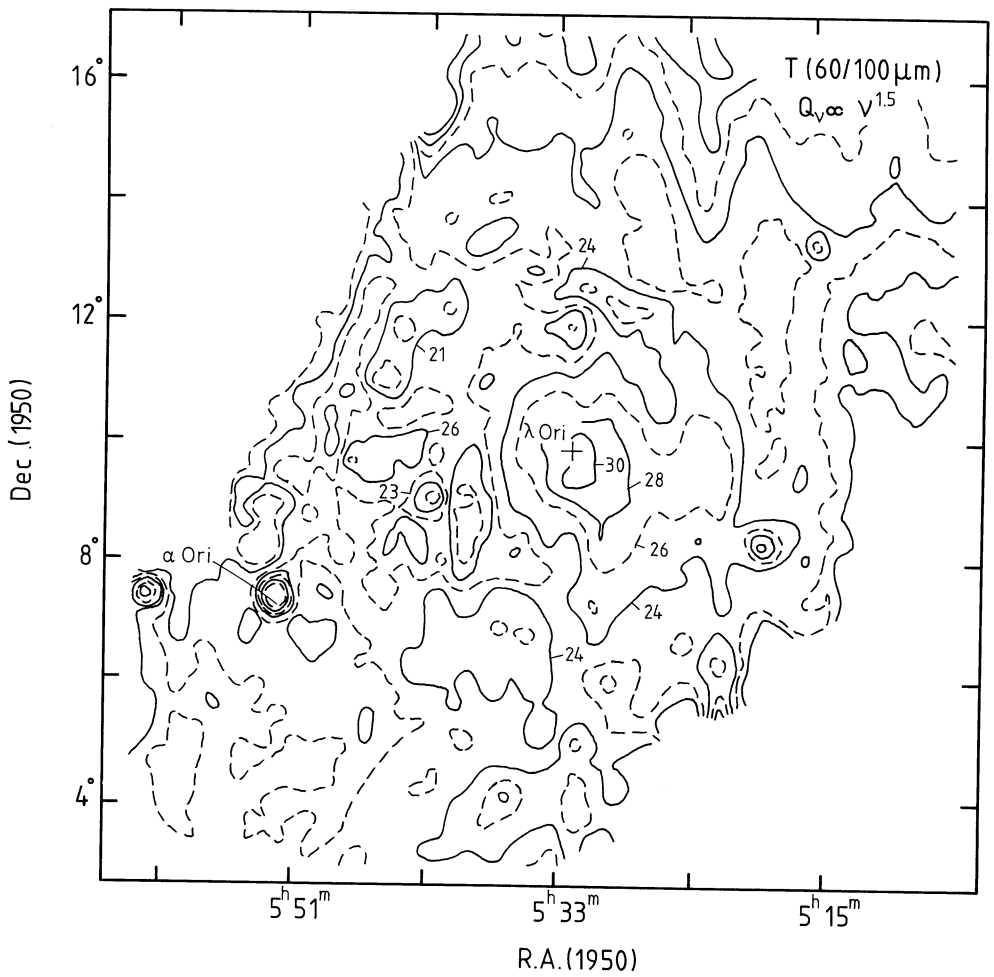

Fig. 4. Map of colour temperature ($I_{60\,\mu m}/I_{100\,\mu m}$ ratio) of the λ Orionis ring and the H II region S 264, assuming a dust emissivity which varies as $\nu^{1.5}$. The contour levels are labelled in units of Kelvin

position angles of $\vartheta = 330°$ and 60°. The ring ends about 4° away from the star λ Ori. In the southeast end of the $\vartheta = 330°$ cut there is infrared emission coming from a crowded region related to the Northern Filament and the Orion B Cloud. Some point-like sources can be seen in the two cuts at 12 and 25 μm. The 100 μm optical depth profiles have a very well-defined shape with strong peaks at the position of the ring.

The flux densities at each wavelength for both the H II region and the dust ring have been obtained by summing the relevant pixels after zero-level correction. The flux densities of several dark clouds in the ring: B35, B223, B31/32, B30, LDN 1582/84, LDN 1583 and B225, have also been derived in the same way. Flux densities and integration areas of all these sources together with those of the ring and S 264 are listed in Table 1. Major error sources are the uncertainties in the calibration and in the background removal. These errors are estimated at about 20% for the 60 and 100 μm bands, and 15% for the shorter wavelength bands. The total observed flux, $F_{8-120\,\mu m}$, has been derived by integrating the measured fluxes from 8 μm to 120 μm (the IRAS wavelength range). To extrapolate to wavelengths outside the IRAS range, we have adopted the result from Boulanger and Pérault (1988) that about 60% of the infrared radiation is emitted within the IRAS wavelength range. The values of $F_{8-120\,\mu m}$ has therefore been multiplied by 1.67 to obtain the total far-infrared flux F_{FIR}. Adopting the distance $d = 400$ pc to the λ Ori OB association (Murdin and Penston, 1977) as the distance to the ring and S 264, we obtained the luminosities $L_{8-120\,\mu m}$ in the IRAS range, and the total far-infrared luminosities, L_{FIR}. These quantities are listed in Table 2.

The mass of the *emitting* dust in the ring has been estimated by summing the 100 μm optical depth pixel by pixel according to the formula:

$$M_d = \varrho_d \sum_i \tau_i \Omega \frac{4ad^2}{3Q_{100\,\mu m}}, \quad (1)$$

where τ_i is the 100 μm optical depth at the i'th pixel, Ω the solid angle of one pixel, d the distance to the ring. The material density of the grains ϱ_d, the grain radius a and the absorption efficiency $Q_{100\,\mu m}$ are taken from Hildebrand (1983). We found a dust mass of 170 $M_\odot$ in the ring. If the mass ratio of gas to dust is 100, then the total mass of gas in the ring associated with the emitting dust is about 1.7 10^4 $M_\odot$. This value may be an underestimate of the true mass, because: (1) the emission is dominated by the hottest grains, consequently cooler grains are not seen; (2) the temperature of the grains emitting most of the 100 μm radiation must be lower than the apparent 60/100 μm color temperature used in deriving $\tau_{100\,\mu m}$ (Terebey and Fich, 1986; Laureijs et al., 1987).

3. Morphology

At all four IRAS wavelengths a ring-like structure is apparent with the star λ Orionis and its surrounding H II region S 264 approximately at its center. The ring is on closer inspection slightly

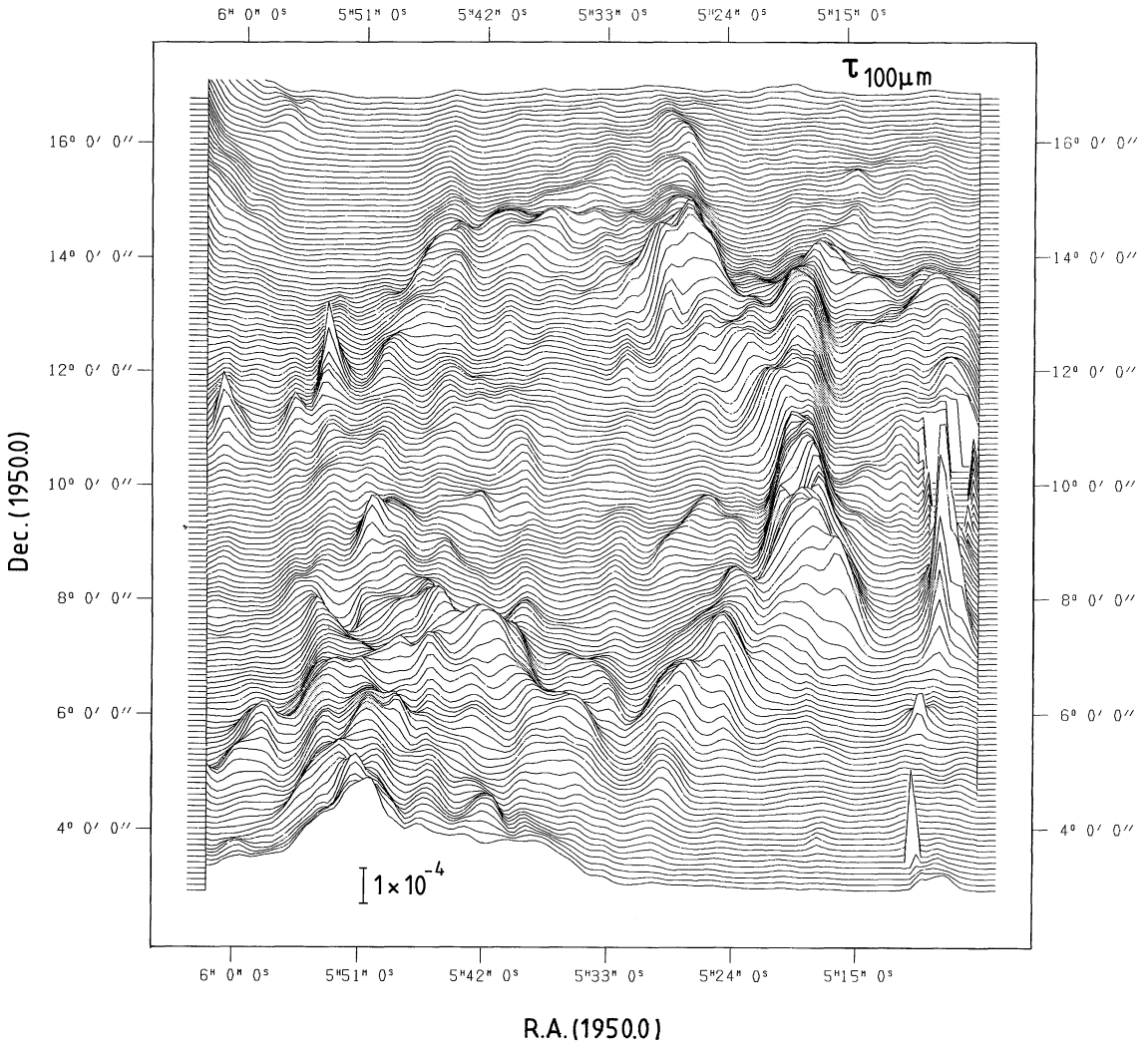

Fig. 5. A ruled-surface plot of the 100 μm optical depth. The vertical line indicates the scale

elongated, and we assume that the observed ellipse is the projection of a circle on the plane of the sky. The following parameters of this circle have been derived from IRAS observations: the radius $r_c = 28.8 \pm 0.7$ pc ($4.^\circ1 \pm 0.^\circ1$), the angle between plane of the sky and plane of the circle is $18.^\circ1 \pm 5.^\circ6$, the line of nodes is at $55.^\circ8 \pm 23.^\circ2$, and the center is at $\alpha = 5^h31^m \pm 1^m$; $\delta = +9°13.'2 \pm 14.'5$.

The ring as seen in infrared emission coincides with the optical opacity ring evident in the extinction map of Khavtassi (1960) and also in the Hα photograph of Isobe (1973). Its center lies about 20′ west and 40′ south of the position of the star λ Ori ($\alpha = 5^h32^m22.^s913$, $\delta = +9°54'8.''35$ [1950]). Although the infrared emission in the IRAS maps traces out a complete ring, the structure is rather inhomogeneous, with less emission observed especially in the northeastern part of the ring.

The existence of a ring is much less obvious in CO data than in the infrared. Nevertheless MM, partly on the basis of kinematic information, fitted a ring to the positions and velocities of the CO peaks MM1 through MM12.They interpret the CO ring as an expanding torus structure with a radial velocity of 6 km s^{-1} and an expansion velocity of 14.3 km s^{-1}. This CO ring does not coincide with the λ Ori dust ring. In particular the CO peaks MM1, MM2, MM3, MM6, and MM7 are located outside the λ Ori dust ring.

The H II region S 264 excited by λ Ori has been observed at 1420 MHz by Reich (1978) He finds an incomplete ring-like structure with λ Ori displaced by about one degree from its center. The infrared morphology of S 264, however, shows a very strong peak close to λ Ori. Also a bar-like structure is visible in the infrared map, at about 2° southwest from the star and extending over $1.^\circ5$. Two peaks at the end of the bar are present at all four IRAS wavelengths. The complex structure of this bar indicates inhomogeneous distribution of internal dust in S 264, but may also be due partly to localized heating within the H II region.

Coulson et al. (1978), on the basis of star counts in the northeastern part of the region centered on λ Ori, conclude that the features around λ Ori can be modeled by a central core of radius 5 pc and two shells of radii 12–14 and 30–33 pc. The inner shell should be visible as a ring in Fig. 1 with a radius of almost exactly 2°. The bar-like structure and the feature observed by Coulson et al. lie indeed on this ring, but about 3/4 of it is not traced out at all. This argues against the existence of the inner shell suggested by Coulson et al. Their outer shell coincides with the

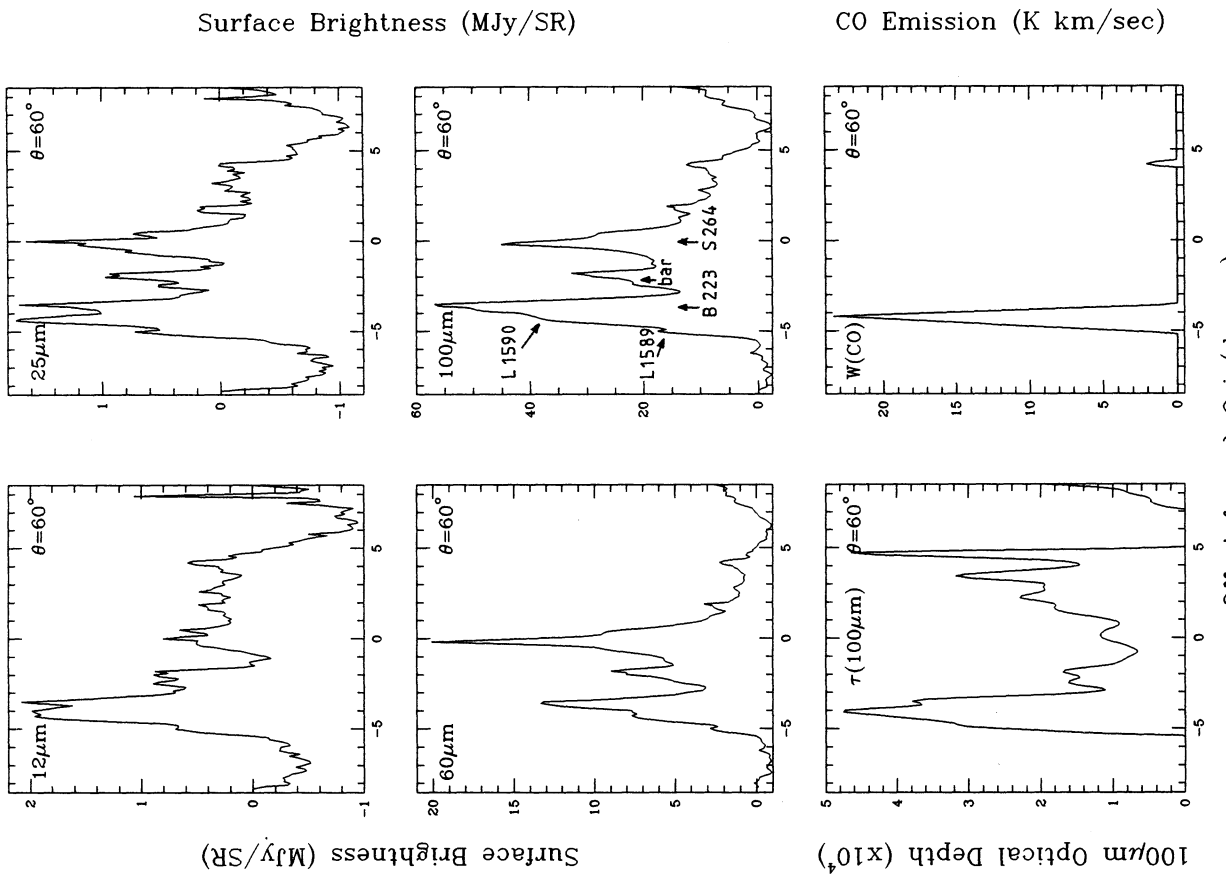

Fig. 6b. A cut through the star λ Orionis with a position angle of 60°. The left side of this cut is roughly towards the southwest. On the 100 μm image (Fig. 1) the cut is indicated by a line BB'. The integrated CO emission W_{CO} is taken from Fig. 1 of MM

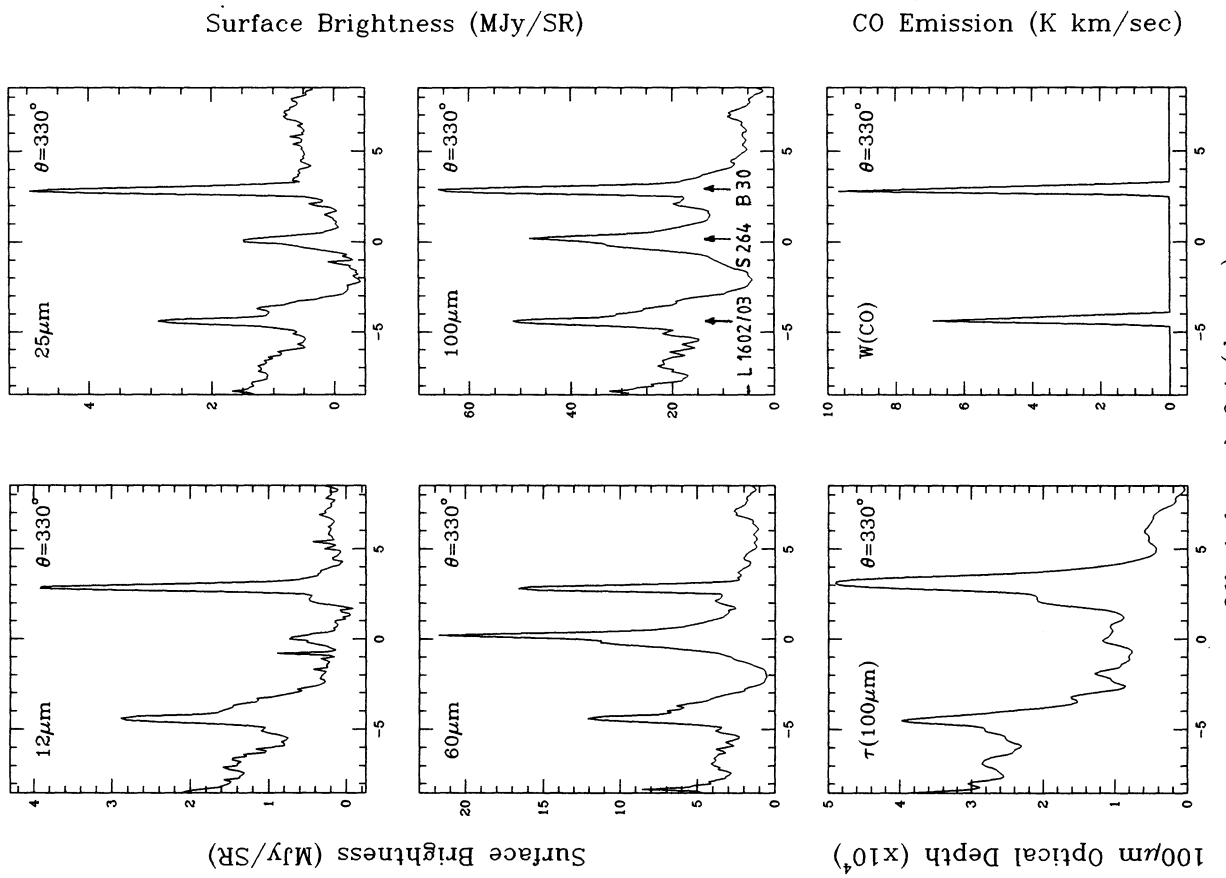

Fig. 6a. A cut through the star λ Orionis with a position angle of 330°. The left side of this cut is roughly towards the southeast. On the 100 μm image (Fig. 1) the cut is indicated by a line AA'. The integrated CO emission W_{CO} is taken from Fig. 1 of MM

Table 1. Infrared flux densities

Source	Flux density (Jy)				Area (10^{-4} sr)
	12 μm	25 μm	60 μm	100 μm	
B35	24	29	160	640	0.85
B223	230	160	2100	5200	2.30
B31/32	41	37	190	630	0.64
B30	150	200	710	2900	1.40
L1582/84	25	40	220	670	0.46
L1583	150	160	570	2000	1.20
B225	19	30	120	300	0.49
Ring	12000	11000	53000	230000	160.00
S264	2500	2400	21000	73000	72.00

Table 2. Total fluxes and luminosities

Source	$F_{8-120\,\mu m}$ (10^{-10} W m^{-2})	$L_{8-120\,\mu m}$ ($L_\odot$)	F_{FIR} (10^{-10} W m^{-2})	L_{FIR} ($L_\odot$)
B35	0.20	100	0.34	170
B223	1.95	990	3.25	1640
B31/32	0.24	120	0.41	210
B30	1.01	510	1.68	850
L1582/84	0.24	120	0.40	200
L1583	0.82	420	0.40	690
B225	0.14	70	0.23	120
Ring	76.0	38000	130.0	63000
S264	22.0	11000	37.0	19000

ring, while the central core can be identified with absorbing dust within S 264, that emits in the far-infrared. Using their model of the distribution of material around λ Ori, Coulson et al. have derived the total extinction of $A_B \approx 1.4 \pm 0.1$ mag and 1.3 ± 0.1 mag for the outer shell and the central core.

More quantitative information on the structures of S 264 and the ring can be obtained by studying two one-dimensional cuts (see Fig. 6a and b) through λ Ori extending 17 degrees. These cuts were made at position angles of $\Theta = 60°$ and $\Theta = 330°$. The central peak in the surface brightness distributions in both cuts indicates emission from the H II region S 264. In the 330° cut two strong peaks outside the central region seen in surface brightness, $\tau_{100\,\mu m}$ and W(CO) correspond to LDN 1602/03 (SE) and B30 (NW), forming parts of the ring. In the 60° cut a peak on the southwest side (left) about 4° away from λ Ori is seen in the surface brightness, $\tau_{100\,\mu m}$ and the CO emission, and is due to the dark cloud B223. Features on the southwest side of this peak are produced by the dark clouds LDN 1589/90. On the northeast side (right), about 4° away from λ Ori, a weak feature is seen in the surface brightness, $\tau_{100\,\mu m}$ and in CO. The peak at 5 degrees northeast away from λ Ori in the optical depth map is probably not real and is due to the combination of cut-off level and noise.

Some of the dark clouds in the ring (B35, B223, and Complex A [B30/31/32/225 and LDN 1582/83/84]) exhibit bright optical rims facing λ Ori (Fig. 2). These are thought to indicate ionization fronts moving from the H II region into the dark, molecular clouds. The clouds also have CO emission ridges near the bright rims, where gas temperatures are enhanced (cf. Fig. 1 of Lada and Black, 1976; Maddalena et al., 1986). We notice that some infrared peaks coinciding with B31/32, LDN 1582/84, and B225 (LDN 1583) lie slightly farther away from λ Ori than the bright rim and seem to form a dust emission ridge (Figs. 1 and 2). This suggests that the increased infrared emission is due to a shock preceding the ionization front; its direct cause being either a density enhancement or increased dust heating by shock-produced ultraviolet photons (see Clark et al., 1986). The last suggestion is not supported by recent CO $J = 1 \rightarrow 0$ observations (Clark, 1988), that show no indication of high-velocity wings in the CO line profiles towards the bright rim near B35. CO is not even detected towards the bright rim regions near LDN 1582/83/84 and B225. It is, however, possible that CO molecules are absent near the ionization front because of dissociation.

The apparent morphology of the ring can be interpreted in two ways: as a torus, suggested for the CO ring by MM, and as a shell, in accordance with the interpretations of Coulson et al. (1978) and Malone et al. (1987). We favor the shell model, because it logically explains infrared features within the ring and because, as explained below, a torus can intercept insufficient energy to account for its emission.

The thickness of the shell, defined as the difference between the outer radius, r_o, and the inner radius, r_i, can be obtained using the ratio of $\tau_{100\,\mu m}$ between peaks in the ring and lowest point near the center of the ring. The ratio, determined from the $\tau_{100\,\mu m}$ distributions in Fig. 6a and b as about 8, leads to the thickness of the shell as 1 pc if a mean radius of the shell is taken to be $r_c = 28.8$ pc (the slight ellipticity of the ring has been disregarded). Since the shell is very thin, we ignore the small correction to the emission of the ring and S 264 listed in Tables 1 and 2, due to part of the shell at the central region near λ Ori.

4. Dust heating

4.1. The ring

4.1.1. Heating agents

The emission from dust heated by the general interstellar radiation field (ISRF) has been extensively studied using IRAS data and several theoretical models have been proposed for the explanation of observed features (Draine and Anderson, 1985; Desert, 1986; Chlewicki and Laureijs, 1988). The ISRF in the local part of the Galaxy has been compiled from direct observations by Mathis et al. (1983). In the λ Ori ring, however, the presence of O and B stars is likely to lead to an enhanced UV component, which has to be taken into account in considering the energy balance of dust grains.

The 60/100 μm intensity ratio $I_{60\,\mu m}/I_{100\,\mu m}$ is 0.23 (the mean color temperature $T(60/100) = 25$ K with a $\nu^{1.5}$ emissivity law) for most of the ring, but it reaches values of 0.25–0.26 ($T(60/100) \approx 26$ K) in some spots associated with B35 and Complex A, and a value as high as 0.38 ($T(60/100) \approx 30$ K) is measured for B223. The typical value of the 60/100 μm intensity ratio for diffuse medium is found to be about 0.2 (Laureijs et al., 1987; Laureijs et al., 1988). A slightly higher value of 0.23 in most parts of the ring is an indication that the radiation field responsible

Table 3. Characteristics of members in the λ Orionis OB association

HD No.	Sp. type	T_{eff} (K)	L_* ($L_\odot$)	L_{UV} ($L_\odot$)
36822	B0 III	30900	20000	13000
36861 [a]	O8 III	34500	150000	90000
36862	B0 V	30900	20000	13000
36881	B8 III	11300	200	60
36894	B9	10700	100	25
36895	B2 V	20500	5500	3600
37035	B9	10700	100	25
37051	B9	10700	100	25
Total			196000	120000

[a] λ Orionis

for dust heating in the ring is enhanced either in the whole spectral range or – more likely in view of the proximity of the O and B stars in the λ Ori association – in the UV wavelength range.

The λ Ori OB association is an obvious source of abundant UV photons. For an O and an early B star the far UV photons in the Lyman continuum are efficiently absorbed by the gas in the H II region. Assuming that a star radiates as a blackbody, the luminosity in the wavelength range from 0.1 to 0.25 μm, L_{UV}, can be estimated as long as its effective temperature, T_{eff}, and total luminosity, L_*, are known. The HD number, the spectral type, T_{eff}, L_* and L_{UV} for eight stars in the λ Ori OB association are listed in Table 3. The spectral types are taken from Murdin and Penston (1977). T_{eff} and L_* for λ Ori are taken from Snow and Morton (1976) and those for the other B stars are from Allen (1973). Summing the contributions from all members of the λ Ori OB association we obtain that the UV energy density in the wavelength range from 0.1 to 0.25 μm at distances of $r = 24$ pc and 30 pc from λ Ori is $L_{UV}/(4\pi cr^2) = 2.2\ 10^{-13}$ and $1.4\ 10^{-13}$ erg cm^{-3}, i.e., two to three times as high as the energy density of the UV component of the general ISRF in the solar vicinity (Mathis et al., 1983).

The above discussion implies that besides the ISRF, the λ Ori OB association does contribute significantly to the heating of the ring, since it raises the energy density in the UV wavelength range, which dominates the heating of grains. In B223, a clump in the ring, associated with the H II region S 263 excited by a B1 V star, HD 34989, the stellar radiation field from this star is responsible for increase of $T(60/100)$ towards the star and the peak color temperature $T(60/100)$ as high as 30 K (the 60/100 μm intensity ratio (0.38) at the position of the star.

4.1.2. Energy balance model

The energy absorbed in the ring will be estimated below. We made the following assumptions for our model calculations. The energy is supplied by the general ISRF and the stellar radiation field from the λ Ori OB association and the star HD 34989. HD 34989 supplies luminosity of about $1.1\ 10^4\ L_\odot$. The total energy longward of 912 Å of the stellar radiation field coming from the λ Ori OB assocoation is summed up to about $1.3\ 10^5\ L_\odot$. Assuming that the ISRF is isotropic and has an energy density $u = 7\ 10^{-13}$ erg cm^{-3} as in the vicinity of the Sun (Spitzer, 1978), the energy flux of the ISRF through a unit surface area is $F_{IS} = uc/4$, where c is the speed of light.

We assume that the ring-like appearance is a projection effect and the actual structure is a dust shell with an outer radius $r_0 = 30$ pc and a thickness of 1 pc as suggested in Sect. 3. The total energy of the ISRF that can be absorbed in the shell is at most $L_{IS} = SF_{IS}$, where the total surface area of the shell $S = 4\pi r_0^2$. The stellar radiation field longward of 912 Å from the λ Ori OB association and the star HD 34989 is almost completely intercepted by the shell. All the quantities: the surface area, S, the energy absorbed from the ISRF, L_{IS}, the energy longward of 912 Å absorbed from the stars, L_s, and the total energy that can be absorbed, $L_{tot} = L_{IS} + L_s$, are given in the last row of Table 4 for the ring. It is found that L_{tot} is a factor of 4.6 larger than the observed far-infrared energy from the ring, and therefore amply sufficient to balance the total energy radiated in the far-infrared.

The amount of energy available for heating the grains would be much smaller for the geometry of a circular torus suggested on the basis of CO data by MM. The circular torus with the dimensions derived from the observed appearance of the ring, i.e., inner radius, $r_i = 24$ pc, outer radius, $r_o = 30$ pc, subtends a solid angle $\Omega = 0.8$ steradian viewed from the λ Ori association. The amount of stellar radiation intercepted by the torus therefore decreases by a factor $\Omega/4\pi = 0.06$ relative to a spherical shell. The total surface area of the torus, which determines the amount of energy intercepted from the ISRF, is about 1/3 of the area of the shell. Using numbers quoted in Table 3, the total available energy for the torus is about 60000 $L_\odot$, and approximately balances the energy emitted in the infrared. The very inhomogeneous structure seen in the infrared and radio maps suggests, however, that the opacity is low over a large portion of the ring, and the energy actually absorbed by dust must be much lower than the total radiative energy available for heating the grains. A torus-like structure is therefore unlikely to capture sufficient energy to balance the infrared emission of the ring. A spherical shell consequently provides a more consistent explanation for all the observed properties of the λ Ori region.

To understand better the energy balance for the individual bright spots in the ring, we have calculated S, L_{IS}, L_s and L_{tot} for the bright spots B35, B223 and Complex A. All these quantities are summarized in Table 4. It is found that the amount of energy that can be absorbed is larger than the observed far-infrared energy, L_{FIR}, from them. The dominant heating source for B223 is HD 34989, which contributes about three quarters of the total energy supply.

Table 4. Energy supply

Source	S (cm^2)	L_{IS} ($L_\odot$)	L_s ($L_\odot$)	L_{tot} ($L_\odot$)
B35	$3.7\ 10^{38}$	510	120	630
B223	$2.1\ 10^{39}$	3000	11500 [a]	14500
Complex A	$2.7\ 10^{39}$	4000	1500	5500
Ring (shell)	$1.1\ 10^{41}$	150000	140000 [a]	290000

[a] Energy supply of $1.1\ 10^4\ L_\odot$ from HD 34989 is included

4.2. S 264

The infrared excess (IRE) of an H II region was first introduced by Mezger (1978), and defined as the ratio between the infrared and Lyman α fluxes ($F_{IR}/F_{Ly\alpha}$). It has long been known that the IRE for H II regions is larger than unity, thus absorption of Lyα photons is not the dominant heating mechanism (see, e.g., Panagia, 1977). Recently Myers et al. (1987) extensively studied associations of H II regions and molecular clouds, and derived that the median IRE of galactic H II regions is 6.

The total far-infrared flux F_{FIR} from the H II region S 264 alone is $3.7\ 10^{-9}$ W m^{-2}. The flux of Lyα photons (in unit of W m^{-2}) is obtained from the optically thin radio continuum flux S_{1420} at 1420 MHz (in unit of Jy). i.e., $F_{Ly\alpha} = 6.6\ 10^{-12} S_{1420}$, where the two-quantum continuum transition is taken into account because of the low electron density in S 264 (see, e.g., Pottasch, 1984). For S 264, $S_{1420} = 185$ Jy (Reich, 1978) leads to IRE = 3.0. The fact that the IRE is larger than unity in S 264 is not surprising and implies that the energy of the Lyα photons is not sufficient to heat the dust grains. Therefore radiation from λ Ori (and possibly from several B stars in the λ Ori OB association) must dominate the heating of dust in S 264. The existence of a temperature gradient in the H II region towards the exciting star (Fig. 4) is consistent with this conclusion.

As found by Ryter et al. (1987), the particles radiating in the 12 μm band are depleted in radiation fields with UV energy density of the order of $u_{UV} = 100$ eV cm^{-3}. A color index $\Gamma_{12} = \nu_1 I_1/(\nu_3 I_3 + \nu_4 I_4)$, where the indices 1 to 4 refers to the four IRAS bands at 12, 25, 60, and 100 μm respectively, was suggested by Ryter et al. (1987). We obtained $\Gamma_{12} = 0.074$ and 0.13 at the position of the emission peak of S 264 and at 4 pc (36′) away from it. The UV energy density of the stellar radiation from λ Ori is greater than 100 eV cm^{-3} at 1 pc from λ Ori and drops to 6 eV cm^{-3} at a distance of 4 pc away from it. This change in the intensity of the 12 μm radiation, which is also directly apparent in the cuts shown in Fig. 6, is therefore consistent with the destruction of particles emitting at 12 μm in strong UV radiation fields suggested by Ryter et al.

5. Conclusions

(1) Infrared maps of the area surrounding λ Ori and the H II region S 264 reveal a ring of dust emission which closely coincides with the structure seen in visual opacity maps. The parameters of the infrared ring differ from those obtained from CO data. The ring has a total mass of at least 20000 solar masses and the emitted energy of 63000 $L_\odot$ in the far-infrared wavelength range.

(2) The radiation field at the location of the ring is enhanced in the ultraviolet wavelength range by a factor of 2 to 3 compared to the UV component of the general ISRF. This is consistent with the presence of the λ Ori OB association and the B1 star HD 34989. The increased UV radiation is responsible for the slightly enhanced avlue of $I_{60\,\mu m}/I_{100\,\mu m} = 0.23$ with respect to galactic cirrus for most parts of the ring.

(3) The energy emitted by the λ Ori OB association, HD 34989 and the ISRF is sufficient to explain the dust heating in the ring. Spherical shell model calculations show that only a fraction (≈20%) of the available radiative energy would have to be absorbed by a shell to explain the emission by the dust in the ring. However, for a circular torus model suggested on the basis of CO data, barely enough energy can be absorbed by the ring to explain its infrared emission. This favors the shell model.

(4) The temperature distribution of dust within S 264 peaks towards λ Ori, and the infrared excess of S 264 is larger than unity (IRE = 3.0). Both facts indicate that the dust within S 264 is heated directly by stellar radiation rather than by Lyα photons in the H II region.

Acknowledgements. We thank our referee, Dr. M. Pérault, for his useful comments and suggestions, which resulted in improvements in the contents of this paper. This work is partially supported by NATO-grant # 0093/88.

References

Allen, C.W.: 1973, *Astrophysical Quantities*, 3rd ed., Athlone Press, London
Barnard, E.E.: 1927, *A Photographic Atlas of Selected Regions of the Milky Way*, eds. E.B. Frost, M.R. Calvert, Carnegie Institution of Washington, Washington, DC.
Boulanger, F., Pérault, M.: 1988, *Astrophys. J.* **330**, 964
Boulanger, F., Baud, B., van Albada, G.D.: 1985, *Astron. Astrophys. Letters* **144**, L9
Chlewicki, G., Laureijs, R.J.: 1988, *Astron. Astrophys. Letters* **207**, L11
Clark, F.O., Laureijs, R.J., Chlewicki, G., Zhang, C.Y., van Oosterom, W., Kester, D.: 1986, *Astron. Astrophys. Letters* **168**, L1
Conti, P.S., Leep, E.M.: 1974, *Astrophys. J.* **193**, 113
Coulson, I.M., Murdin, P.G., MacGilliverey, H.T., Zealey, W.J.: 1978, *Monthly Notices Roy. Astron. Soc.* **184**, 171
Desert, F.X., Boulanger, F., Shore, S.N.: 1986, *Astron. Astrophys.* **160**, 295
Draine, B.T., Anderson, N.: 1985, *Astrophys. J.* **292**, 494
Duerr, R., Imhoff, C.L., Lada, C.J.: 1982, *Astrophys. J.* **261**, 135
Hildebrand, R.H.: 1983, *Quart. J. Roy. Astron. Astrophys.* **24**, 267
Hoffleit, D., Jaschek, C.: 1982, *The Bright Star Catalog*, Yale University Observatory
Isobe, S.: 1973, IAU Symposium **52**, *Interstellar Dust and Related Topics*, eds. J.M. Greenberg, H.C. van de Hulst, Reidel, Dordrecht, p. 433
IRAS Catalogs and Atlases, Explanatory Supplement 1985, U.S. Government Printing Office, Washington, DC
Khavtassi, D.S.: 1960, *Atlas of Galactic Dark Nebulae*, Abstumanskaya Astrofiz. Observatory
Lada, C.J., Black, J.H.: 1976, *Astrophys. J. Letters* **203**, L75
Laureijs, R.J., Mattila, K., Schnur, G.: 1987, *Astron. Astrophys.* **184**, 269
Laureijs, R.J., Chlewicki, G., Clark, F.O.: 1988, *Astron. Astrophys. Letters* **192**, L13
Low, F.J., Beintema, D.A., Gautier, T.N., Gillett, F.C., Beichman, C.A., Neugebauer, G., Aumann, H.H., Baud, B., Boggess, N., Emmerson, J.P., Habing, H.J., Hauser, M.G., Houk, J.R., Rowan-Robinson, M., Soifer, B.T., Walker, R.G., Wesselius, P.R.: 1984, *Astrophys. J. Letters* **278**, L19
Maddalena, R.J., Morris, M., Moscowitz, J., Thaddeus, P.: 1986, *Astrophys. J.* **303**, 375
Maddalena, R.J., Morris, M.: 1987, *Astrophys. J.* **323**, 179
Malone, D., MacBreen, B., Fazio, G.G.: 1987, *Irish Astron. J.* **18**, 91
Mathis, J.S., Mezger, P.G., Panagia, N.: 1983, *Astron. Astrophys.* **128**, 211
Mezger, P.G.: 1978, *Astron. Astrophys.* **70**, 565
Murdin, P., Penston, M.V.: 1977, *Monthly Notices Roy. Astron. Soc.* **181**, 657

Myers, P.C., Dame, T.M., Thaddeus, P., Cohen, R.S., Silverberg, R.F., Dwek, E., Hauser, M.G.: 1986, *Astrophys. J.* **301**, 398
Panagia, N.: 1977, *Infrared ans submillimeter Astronomy*, ed. G.G. Fazio, Reidel, Dordrecht, p. 43
Pottasch, S.R.: 1984, *Planetary Nebulae*, Reidel, Dordrecht
Reich, W.: 1978, *Astron. Astrophys.* **64**, 407
Ryter, C., Puget, J.L., Pérault, M.: 1987, *Astron. Astrophys.* **186**, 312
Sharpless, S.: 1959, *Astrophys. J. Suppl.* **4**, 257
Snow, T.P., Morton, D.M.: 1976, *Astrophys. J. Suppl.* **32**, 429
Spitzer, L.: 1978, *Physical Processes in the Interstellar Medium*, *Chapter 9*, Wiley, New York
Terebey, S., Fich, M.: 1986, *Astrophys. J. Letters* **309**, L73
Wade, C.M.A.: 1957, *Astron. J.* **62**, 148
Wade, C.M.A.: 1958, *Rev. Modern Physics* **30**, 946
Weiland, J.L., Blitz, L., Dwek, E., Hauser, M.G., Magnani, L.: 1986, *Astrophys. J. Letters* **306**, L101